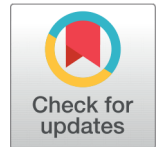


# CORRELATION BETWEEN MICROSTRUCTURAL AND CORROSION RESISTANCE OF BORON-MODIFIED DUPLEX STAINLESS STEEL PROCESSED BY SPRAY-FORMING



Moises Meza Pariona<sup>1</sup>  

<sup>1</sup>Department of Materials Engineering, State University of Ponta Grossa, Ponta Grossa-PR, Brazil



## ABSTRACT

In this work was investigated the duplex stainless steel modified by boron processed by spray-forming, in order to characterize the workpiece using different techniques, optical microscopy, SEM-FEG, X-ray diffraction, Rama spectroscopy and Vickers hardness (VH) and Thermo-Calc software, with goal of determining the corrosion resistance. The corrosion resistance test was performed in aerated solution of 0.1 M, immersed in different aggressive media electrolytes, alkaline and acidic mediums. As result through the EDS technique was verified that in the ferrite phase the Cr element predominates, but in the austenite phase the Fe and Ni elements prevail. Meanwhile XRD spectra shown different meta-stable phases and mainly the  $(\text{FeCr})_2\text{B}$  phase, the percentage of the austenite and ferrite phases are similar. Besides, the Vickers microhardness measurement was around 460 HV. Furthermore, Nyquist impedance plots at different electrolytes had linear behavior, which their polarization resistances are extremely high in all solutions. However, the potential of corrosion whose magnitude is small, also the corrosion rates were close to zero. Consequently, the corrosion resistance in all studied solutions were extremely high and it can be attributed due to presence of the  $(\text{FeCr})_2\text{B}$  phase, meta-stables phases and similar proportion of the three phases present. This alloy can be successfully used in the chemical, oil and gas industries and petrochemical process plants.

Received 6 May 2021  
Accepted 20 May 2021  
Published 31 May 2021

**Corresponding Author**  
Moises Meza Pariona, [mmpariona@uepg.br](mailto:mmpariona@uepg.br)

DOI [10.29121/granthaalayah.v9.i5.2021.3934](https://doi.org/10.29121/granthaalayah.v9.i5.2021.3934)

**Funding:** This research received no specific grant from any funding agency in the public, commercial, or not-for-profit sectors.

**Copyright:** © 2021 The Author(s). This is an open access article distributed under the terms of the Creative Commons Attribution License, which permits unrestricted use, distribution, and reproduction in any medium, provided the original author and source are credited.

**Keywords:** Boron-Modified Duplex Stainless Steel, Spray-Forming, SEM-FEG, Vickers Hardness, XRD, Rama Spectroscopy, Corrosion Resistance

## 1. INTRODUCTION

Traditional stainless steels do not present the adequate combination of mechanical resistance and pitting corrosion, necessary in a series of applications, mainly in the presence of sea water, as is the case of equipment used in offshore platforms. Nevertheless, there are a relatively new category of stainless steels, called duplex



and super duplex, satisfactorily combines these characteristics, as reported by Bernhardsson [Charles et al. \(1991\)](#). However, Martins [Martins \(2006\)](#) pointed out that success in cast in duplex and super duplex is mainly related to the precipitation of the sigma phase during cooling after solidification and this intermetallic significantly reduces the toughness of the material. The sigma phase precipitates at the ferrite/austenite interfaces and grows toward the ferrite, it requires alloying elements (chromium and molybdenum) for its formation. In addition, American Society For Testing And Materials “[Standard Practice For Castings, Iron-Chromium-Nickel-Molybdenum Corrosion Resistant, Duplex \(Austenitic/Ferritic\) For General Application](#)” (1999) and Smuk [Li et al. \(2016\)](#) reported that the sigma phase is not the only intermetallic phase that precipitates into the microstructure of these alloys; other phases such as: phase “Chi” ( $\chi$ ), phase “R”, phase “G”, phase “Tal” ( $\tau$ ), etc. High alloy duplex stainless steels: commonly referred as super duplex, denoted as UNS S32750 (SAF 2507) presents high resistance to corrosion comparable to the super austenitic that possess between 5 and 6% of molybdenum.

Super duplex stainless steel (SDSS) consists primarily of chemical concentrations of chromium, nickel, molybdenum and nitrogen. Chemical composition (wt. %) of super duplex 2507: C, max 0.003; Cr, 25; Ni, 7; Mo, 4 and others. One way to empirically quantify that chemical property is through the equivalent resistance to pitting corrosion, or PREN (Pitting Resistance Equivalent). According to ASTM A890/A890M “[Standard Practice For Castings, Iron-Chromium-Nickel-Molybdenum Corrosion Resistant, Duplex \(Austenitic/Ferritic\) For General Application](#)” (1999), this magnitude can be calculated from the expression:

$$\text{PREN} = \%Cr + [(3,3) \times (\%Mo)] + [(16) \times (\%N)]. \quad (1)$$

Thus, the biphasic stainless steels (ferritic/austenitic) whose PREN values are in the range of 35 to 40, constitute the family of duplex stainless steels and for PREN greater than 40, constitute the family of super duplex stainless steels, this alloy exhibits mechanical strength, corrosion resistance, and toughness at low temperatures, being superior to common duplex stainless steels. It has high resistance to pitting corrosion and chloride-containing environments. It is mainly used on offshore platforms for oil and gas extraction, such as in pumps, valves, flanges and pipelines. An important study given by Li et al. [Li et al. \(2016\)](#) remarked, which duplex stainless steel (DSS) is widely used in various industries due to its combination, such as, excellent properties mechanical and corrosion resistance.

Zepon et al. [Zepon et al. \(2016\)](#) emphasized that Spray Forming (SF) process consists in atomizing of a liquid metal jet in multi-drop with varying size and which it is driven by inert gas at high speed, ranging typically is from  $10^2$  to  $10^5$   $\text{Ks}^{-1}$ , however, before they reach the substrate, the metal droplets are cooled at high rates, moreover, the trajectory of these drops is interrupted by a substrate in which they solidify in the form of a coherent deposit and with characteristics close to the theoretical density.

Meanwhile, by means of SF technique enables achievement of refined microstructures with low segregation level, supersaturated solid solutions with meta-stable phases or even the formation of amorphous phases. Therefore, an application of this study by SF process was in solidification of boron-modified super martensitic stainless steel (BSMSS) at 0.3 to 0.7 wt% B, aiming in to increase the wear resistance of BSMSS and achieved a refined microstructure, free of macro segregations, consisting of a uniform equiaxial structure of the matrix, where finely dispersed carbides were present. In previous work, Soyama et al. [Soyama et al. \(2019\)](#) studied wear resistant in boron-modified duplex stainless steels processed by spray forming, where the wear resistance was evaluated for these steels in the dry sand/rubber wheel test. Consequently, the wear resistance for boron-containing steels had a significant improvement in comparison with the same steel without boron. This improvement was attributed to the presence of fine and well-distributed boride particles that protected the austenitic-ferritic matrix from material removal.

An important study by Soyama et al. [Soyama et al. \(2019\)](#), since one of the greatest advantages of borides lies in the fact that boron has a very limited solubility in ferrite and austenite, consequently, boride formation occur during solidification and that two different boride phases can be identified:  $M_2B$  and  $M_3B_2$  ( $M = Fe, Cr, Mo$ ). Considering that boron has a limited solubility in ferrite, as ferrite grains are formed in equilibrium conditions, boron remains in the liquid phase and thus is segregated to the grain boundaries, furthermore, when the eutectic point is reached,  $M_2B$  becomes stable and forms by reacting with Fe and Cr resulting in the continuous network of borides.

Chail and Kangas [Chail and Kangas \(2016\)](#) discussed, which hyper duplex stainless steels have the highest critical pitting temperature, and critical crevice corrosion temperature than the modern duplex stainless steels. Hyper duplex stainless steels have the highest tensile and fatigue strengths among the modern duplex stainless steels. With these combinations of extreme high corrosion resistance and strength, hyper duplex stainless steels can be successfully used in the extreme oil and gas environments in the ultra-deep formations or deep-water wells.

In this work the purpose was investigating corrosion resistance in alkaline and acidic mediums of the duplex stainless steels with addition of 2.0 wt% B, which it was processed by spray-forming and whose workpieces were characterized by different techniques, optical microscopy, SEM-FEG, X-ray diffraction, Rama spectroscopy and Vickers hardness (VH), Thermo-Calc software and electrochemical techniques. The corrosion resistance test was performed in aerated solution of 0.1 M, immersed in alkaline and acidic mediums aggressive, to study the applicability of this steel in these mediums.

## 2. MATERIALS AND METHODS

The mixture of the raw materials (Table 1) with adjusted composition was melted in an induction furnace using an alumina crucible, subsequently, SF process was applied in nitrogen gas with an atomization pressure of 0.5 MPa and the pouring temperature was approximately 1650 °C. The deposition was carried out on a mild steel substrate, resulting as an end-product a disc of approximately 3.5 kg with 300 mm in diameter and 25 mm in thickness.

Characterization of the boron-modified duplex stainless steels (BDSS) samples was performed using different techniques. Therefore, the microstructure was analyzed by a Shimadzu SSX-550 SEM-FEG microscopy and coupled to the dispersive energy spectroscopy (EDS) mapping and an Olympus BX-51 optical microscope (OM) with a QColor 3 digital camera for the image capture. As well, X-ray diffraction (XRD) analysis were recorded at a scan speed of 0.2° min<sup>-1</sup>, using a Rigaku mark equipment, model: Ultima IV, X-ray diffractometer with power 40/30 kW; besides, Xplora plus Raman microscope - Bruker Snterra equipment, with wavelength 532 nm (green) and with beam power 0.2 mW; furthermore, to measure the hardness of the material a Micro Vickers Hardness (VH) Tester was used, applied 1000 [gF] for a time of 15 [s]. The corrosion test was performed in aerated solution of 0.1 M, immersed in different electrolytes: Sulfuric acid (H<sub>2</sub>SO<sub>4</sub>), sodium sulfate (Na<sub>2</sub>SO<sub>4</sub>), sodium chloride (NaCl), sodium carbonate (Na<sub>2</sub>CO<sub>3</sub>) and sodium hydroxide (NaOH) at a temperature of 25°C ± 0.5°C. Working electrodes of surface-treated and untreated samples were prepared with epoxy resin. Corrosion potentials (E<sub>cor</sub>) were measured using Autolab PGSTAT 30 potentiostat system connected to a microcomputer. Beraha's tint reagent was used for sample attack, with composition of 200 mL HCl and 1000 mL H<sub>2</sub>O and 0.5 g K<sub>2</sub>S<sub>2</sub>O<sub>5</sub> for about 60 seconds. In Table 1 is shown the elements concentration of boron-modified hyper duplex stainless steel in wt.% by fluorescence spectroscopy

**Table 1** Fluorescence spectroscopy data of boron-modified duplex stainless steel

Element	Wt. %
Fe	64.3
Cr	27.0
Mo	3.0
Ni	3.0
B	2
C	0.06
N	0.1

### 3. RESULT AND DISCUSSION

#### 3.1 SURFACE CHARACTERIZATION

##### 3.1.1 MICROSTRUCTURAL ANALYSIS BY MICROSCOPY

In this chapter the results of microstructure, ray-x, Raman spectroscopy, microhardness, and corrosion resistance by electrochemical techniques of BYDSS workpiece will be shown and discussed.

According to Equation (1) and Table, the PREN value was calculated, whose value was 38.5, so this value is in the range of 35 and 40, as it was established by the standards “Standard Practice For Castings, Iron-Chromium-Nickel-Molybdenum Corrosion Resistant, Duplex (Austenitic/Ferritic) For General Application” (1999), it constitutes the family of duplex stainless steels belong to Fe-Ni-Cr system. Addition of Mo is mainly to improve corrosion resistance, but also increase the strength. Addition of N is mainly to increase strength but also improve structure stability and corrosion resistance, as emphasized by Chail and Kangas [Chail and Kangas \(2016\)](#), as well as the boron, is also present in this type of steel. So, in this work the material is boron-modified duplex stainless steels (BDSS) that was used for this study.

Usually when the super duplex stainless steel does not have boride, the authors [Sharafi \(1993\)](#), Wang et al. [Wang et al. \(2011\)](#), Emami et al. [Emami et al. \(2018\)](#), Martins and Casteletti [Martins and Casteletti \(2005\)](#), Smuk [Smuk \(2004\)](#) and Arun et al. [Arun et al. \(2019\)](#) confirmed two types of phases, austenite and ferrite and they reported that duplex stainless steel is the name given to the class of materials with biphasic microstructure, it is composed of a ferritic matrix and austenite islands, with volumetric fractions of approximately 50% of each phase.

Duplex stainless steels are a group of stainless steels with a microstructure of almost equal amount of austenite and ferrite. These materials show an attractive combination of excellent corrosion resistance and high mechanical properties comparing with either austenitic stainless steels or ferritic stainless steels, especially super duplex stainless steels, as evidenced by Chail and Kangas [Chail and Kangas \(2016\)](#).

The phase diagrams of BDSS by the thermodynamic simulation, using ThermoCalc software [Software \(2017\)](#) is shows in [Figure 1](#), where an investigation of stable phases and metastable phases containing high level of boron was conducted in this study. According to Soyama et al. [Chail and Kangas \(2016\)](#), which boride formation in super duplex stainless steels occur during solidification and two different boride phases can be identified,  $M_2B$  and  $M_3B_2$  ( $M = Fe, Cr, Mo$ ). In [Figure 1](#), we can clearly observe the presence of the ferrite and austenite, in addition, other principal phases precipitate occurs, boride phases ( $M_2B$  and  $M_3B_2$ ), chromium carbide and sigma phase from 1200 to 600°C. Considering the proportion of phase areas in [Figure 1](#), as much as for austenite and ferrite was stipulated approximately these areas in 30%. A similar result was found in ref. [Chail and Kangas \(2016\)](#).

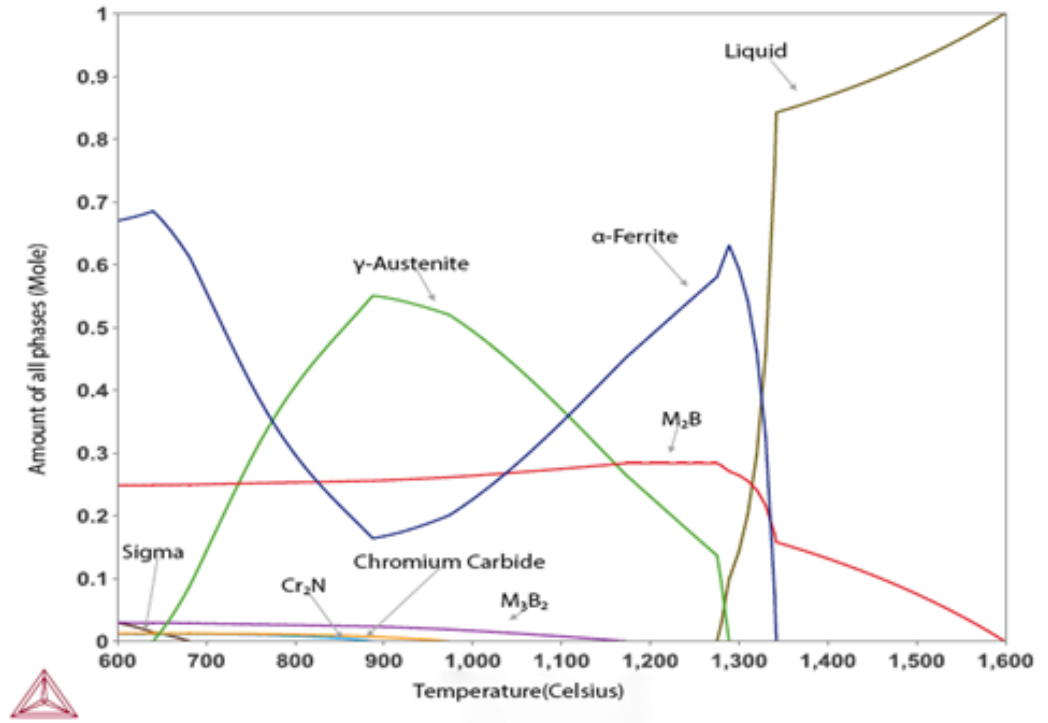


**Figure 1** Phasediagram of a boron-modified duplex stainless steel

The general view of the cross section of alloy is shown in [Figure 2](#) , where can be observed the austenite and ferrite in approximately equal fractions and borides is embedded in a matrix (stipulated approximately in 30%, according to the corresponding area in [Figure 1](#) . This microstructure is shown at different magnifications by optical microscopy in [Figure 2](#) a-b, exhibiting the borides morphology in blocky-shaped as a branching of the ferrite [Soyama et al. Chail and Kangas \(2016\)](#), they pointed out, which considering that boron has a limited solubility in ferrite, as ferrite grains are formed in equilibrium conditions, boron remains in the liquid phase and thus is segregated to the grain boundaries, furthermore, when the eutectic point is reached, Melongated lamellae is a branch of the ferrite and however austenite has a diffuse feature as can be verified in this work ([Figure 2](#) ).

[Martins \(2006\)](#) confirmed that in the duplex and super duplex stainless steels obtained by casting process in sand molds, it is almost impossible to prevent sigma phase precipitation during solidification due to low cooling speed. Furthermore, this authors point out that the success in obtaining components cast in duplex and super duplex stainless steel is mainly related to exercising effective control over the precipitation of the sigma phase during cooling in solid state (especially in the range 800-500°C), as this intermetallic significantly reduces the toughness and corrosion resistance of the material. However, by Spray Forming (SF) process, [Zepon et al. \(2016\)](#) obtained a refined microstructure during solidification, free of

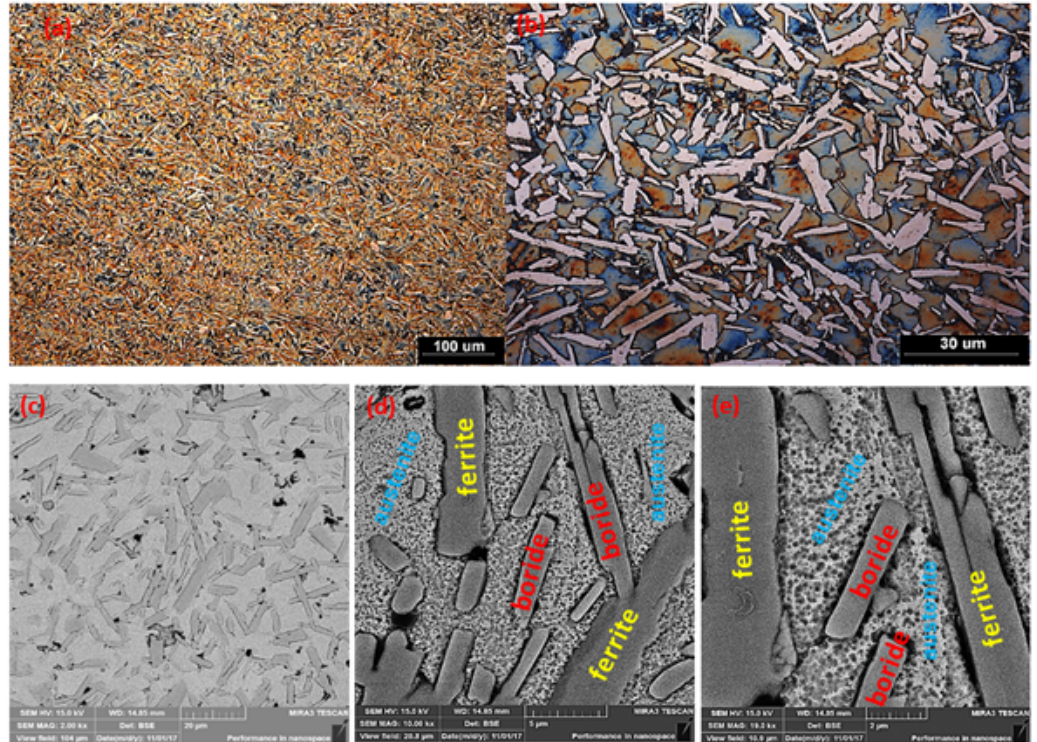


**Figure 2** The top-view of a sample by optical and SEM images. a) Optical micrograph, b) Optical micrograph with more magnification of previous one and c) SEM micrographs of alloy, d) and e) with higher magnification of c).

macro segregations, consisting of a uniform equiaxed structure of the matrix. Therefore, through this technique it is possible to avoid the sigma phase that originates in the traditional casting, such as using sand mold. These latter authors state, in SF process the metal droplets are cooled at high rates, the ranging typically from  $10^2$  to  $10^5$   $\text{Ks}^{-1}$ , thus it generates high rates of solidification and although, in sand mold the solidification is of low cooling speed.

### 3.2 MICROSTRUCTURAL ANALYSIS BY SEM/EDS

For a compositional analysis of different elements in the sample, the energy dispersive X-ray spectroscopy (EDS) was used, in conjunction with SEM to provide high-superficial resolution imaging. In image of [Figure 3](#) are observed the microstructures  $\gamma$ -austenite (blue) with diffuse characteristic,  $\alpha$ -ferrite with elongated lamellae characteristic (yellow) and boride (red) with faceted and elongated characteristic.

For these analyses, in the micrograph were considered four-point, for measurements of the elements in the austenite, ferrite and boride phases and in table on the right side shows the elements and the standard deviation ( $\sigma$ ). At result of point analysis by EDS, at the ferrite phase there is more Cr than at the boride and austenite phase, although, this element prevails in boride than in austenite, however, at

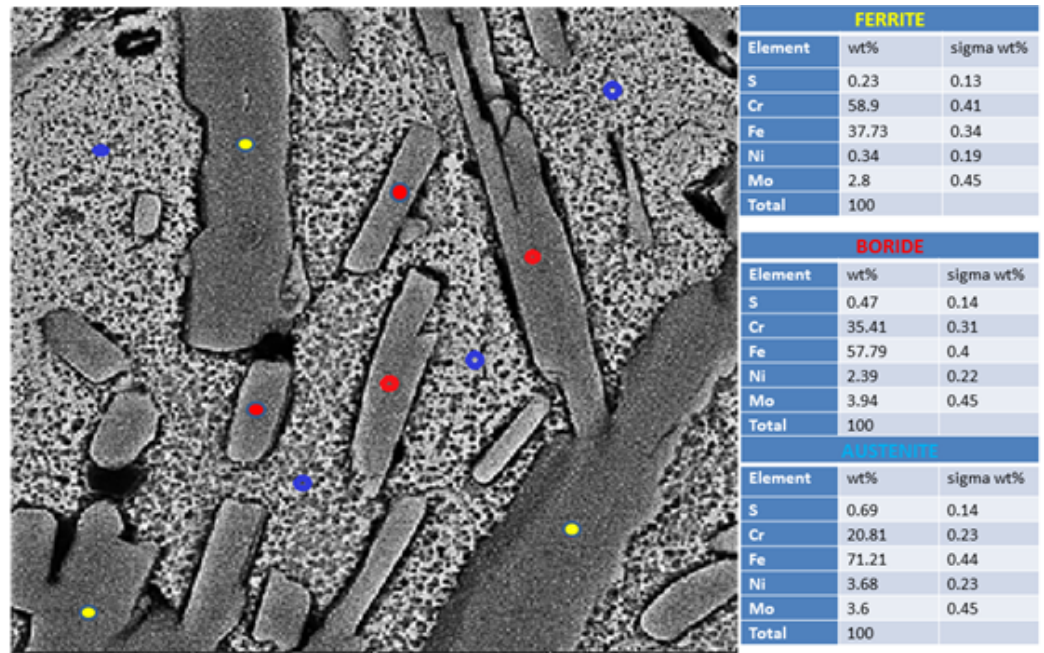


Figure 3 SEM image of BDSS surface and EDS punctual analysis

the austenite phase there is more concentration of the Fe, Ni, and S elements than at the ferrite and boride phases, nevertheless, Fe prevails in boride and lastly in ferrite. Considering the tables in Figure 3, the boride phase is rich in Fe and Cr, thus identifying, which the  $M_2B$  phase (Figure 1) correspond to the  $(FeCr)_2B$  phase. However, in this study the boron element was not identified by this technique. Furthermore, the EDS spectra analysis in a region was performed, which is shown in Figure 4.

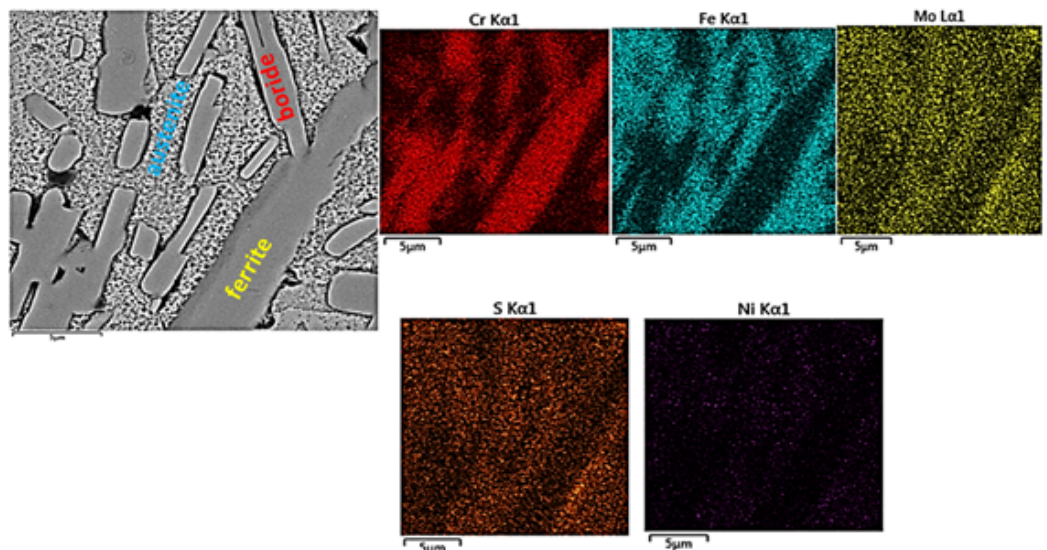
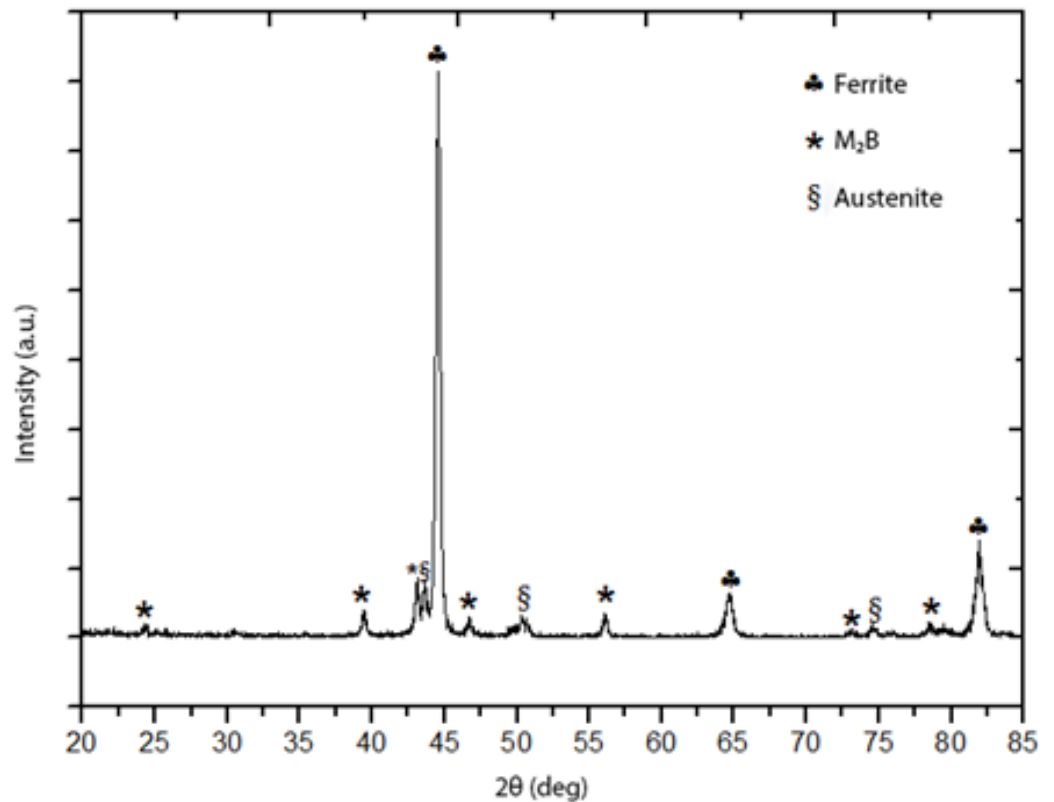


Figure 4 TheEDS spectra analysis in a region at BDSS workpiece

According to EDS spectra (Figure 4) in the analysis region are presents different elements, where there is a higher concentration of Cr at ferrite and followed in the borides, which is verified by point analysis (Figure 3). However, the elements Fe, Ni and S have higher concentration in the austenite phase; nevertheless, Fe also has a high concentration in the boride phase. So again, this result is verified with the point analysis.

This analysis corroborated our study by EDS punctual analysis and EDS spectra analysis in a region, having a high concentration of Cr in the ferrite phase and followed in the boride phase, thus, the existence of the borides of type  $(\text{FeCr})_2\text{B}$  phase was also verified by Thermo-Calc and in the microstructure.



**Figure 5** XRD spectra of BDS with 2 wt.% B

### 3.3 X-RAY DIFFRACTION (XRD)

Moreover, in this work BDS was investigated by X-ray diffraction analysis (XRD) that is shown Figure 5, the standard XRD patterns of different metallic elements were identified, such as, Cr, Fe, Ni and meta-stable phases, Fe-Cr, FeNi,  $\text{Cr}_{0.19}\text{Fe}_{0.7}\text{Ni}_{0.11}$ , Ni-Cr-Fe and  $\text{Cr}_{1.36}\text{Fe}_{0.52}$ , most of these phases are concentrated at the peak of greatest intensity, accompanied by the ferrite phase. In addition, some of these metallic elements and meta-stable phases, austenite and  $\text{M}_2\text{B}$  or  $(\text{FeCr})_2\text{B}$  phases also

are found in other peaks of lower intensity, as it can be seen in Figure 5. The formation of these meta-stable phases is promoted by the high speed of cooling generated in the spray-forming process, which leads to the formation of the ferrite, austenite, and boride phases (Figure 1). Kashiwar et al. Software (2017) found that in the 2-theta between 44 and 45 degrees the main peaks of the austenite and ferrite phases are presented, in this way our work is confirmed. Thus, the  $(\text{FeCr})_2\text{B}$  phase was verified that to exist in BDSS by XRD and Thermo-Calc techniques.

### 3.4 RAMAN SPECTROSCOPY

The corresponding Raman spectra result is shown in Figure 6. The strong peaks is located at  $\sim 492 \text{ cm}^{-1}$ , followed by  $2443 \text{ cm}^{-1}$ , however other smaller peaks are around of  $537 \text{ cm}^{-1}$ ,  $1198 \text{ cm}^{-1}$ ,  $1468 \text{ cm}^{-1}$ ,  $1532 \text{ cm}^{-1}$ ,  $1619 \text{ cm}^{-1}$  and  $1773 \text{ cm}^{-1}$ . The peaks  $492$  to  $537 \text{ cm}^{-1}$  are in range accordingly with Ran et al. Ran et al. (2015), which they have studied duplex stainless steels (DSSs)  $19\text{Cr}-10\text{Mn}-0.3\text{Ni}-x\text{N}$  ( $x = 0.211-0.315 \text{ wt.}\%$ ) and as well as, also, in agreement with Xu et al. Xu et al. (2012), who investigated Raman spectra obtained by spotting a laser beam on different regions of the oxide film introduced on DSS  $25\text{Cr}-10\text{Mn}-2\text{Ni}-3\text{Mo}-0.8\text{W}-0.8\text{Cu}-0.5\text{N}$  oxidized. Mironova-Ulmane et al Mironova-Ulmane et al. (2011) studied nickel oxide by Raman scattering, which the found peak in the range of  $110$  to  $1500 \text{ cm}^{-1}$ , due to this fact, we could attribute in this range the presence of Ni and other meta-stable phases with Ni, this result corroborates with x-ray spectrum (Figure 5). No further information was found because Raman spectroscopy is still poorly studied in BDSS.

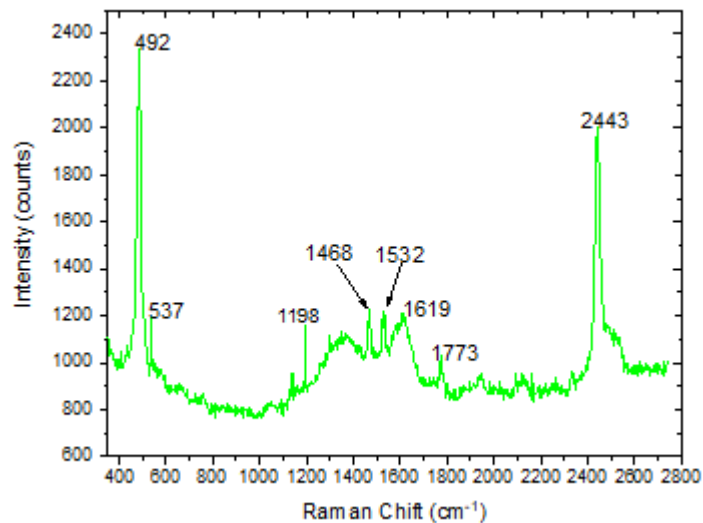


**Figure 6** Raman spectra of BDSS with 2 wt.% B

### 3.5 VICKERS MICROHARDNESS MEASUREMENTS

The study of Vickers microhardness measurements in BDSS workpiece were carried out in this research. In this work the Vickers microhardness test was applied. As result, the microhardness Vickers (HV) was 460 with standard deviation of 14.7.

Sousa et al. [Souza et al. \(2010\)](#) reported that the material analyzed for super duplex stainless steel alloy exhibited a Vickers microhardness (HV) average value of 261 for austenite and 305 HV for ferrite, however, Bastos et al. [Bastos et al. \(2007\)](#) for same material presented a hardness value of 278 HV and besides, Deng et al [Deng et al. \(2009\)](#) reported that Vickers hardness values for UNS S31803 duplex stainless steel in the range of 249–254HV. Meanwhile, in this study Vickers microhardness measurements was around 460 HV, being much higher measured by the authors presented, this fact justifies, that this material was processed by Spray Forming (SF) technical, since, this technique promotes refined microstructures with low segregation level, supersaturated solid solutions with meta-stable phases (to see [Figure 5](#)) or even the formation of amorphous phases, as affirmed by Zepon et al. [Zepon et al. \(2016\)](#) and Soyama et al. [Soyama et al. \(2019\)](#), still these authors highlight and confirm, which the high microhardness can mainly be attributed to the existence of borides of type  $(\text{FeCr})_2\text{B}$ , this result confirms our work, thus, in boron-modified duplex stainless steel processed by spray-forming contain this phase, which were verified by XRD spectra and Thermo-Calc software.

### 3.6 CORROSION BEHAVIOR OF BDSS IN DIFFERENT ELECTROLYTES

#### 3.6.1 OPEN CIRCUIT POTENTIAL VERSUS TIME

To quantify the corrosion rate of this steel was calculated the open circuit potential (OCP), which was determined after 3300 seconds when the material is immersed in an electrolyte, according to the standard [Pehkonen and Yuan \(2019\)](#). Where OCP of an electrode in the electrochemical corrosion inform us about the thermodynamic tendency in the electrolyte or neighboring medium. As result, Table 2 shown the OCP represented by Ecorr of boron-modified duplex stainless steel sample, at 0.1 M of sulfuric acid ( $\text{H}_2\text{SO}_4$ ), sodium sulfate ( $\text{Na}_2\text{SO}_4$ ), sodium chloride (NaCl), sodium carbonate ( $\text{Na}_2\text{CO}_3$ ), sodium hydroxide (NaOH). The electrode in some solutions showed noble behavior in concerning to other solutions. For example, the workpiece was nobler in NaCl than in  $\text{Na}_2\text{SO}_4$ , followed by  $\text{H}_2\text{SO}_4$ ,  $\text{Na}_2\text{CO}_3$ , and NaOH. This means that the workpiece was less noble at the NaOH solution. In a general manner, it should be noted that all the OCP potentials of the workpiece are quite similar.

#### 3.6.2 POLARIZATION CURVES

The corrosion rate is related to polarization resistance ( $R_p$ ) measurements, it is used to determine the protection capability in a given solution. The polarization resistance ( $R_p$ ) is obtained by the linear polarization resistance method, for this case, current linearly depends in a narrow potential region, well the,  $E_{\text{corr}} = \pm 10$  mV.

$R_p$  is the slope of the experimental E versus i curve at  $E_{corr}$ , which according to the Stern–Geary relationship is calculated. The following are shown the equation proposed by Pehkonen et al. [Pehkonen and Yuan \(2019\)](#).

$$R_p = \left( \frac{dE}{di} \right)_{E_{corr}} = \frac{\beta_a \beta_c}{2.3 i_{corr} (\beta_a + \beta_c)} \quad (2)$$

$$i_{corr} = \frac{\beta_a \beta_c}{2.3 R_p (\beta_a + \beta_c)} = \frac{B}{R_p} \quad (3)$$

$$B = \frac{1}{2.3 \left( \frac{1}{\beta_a} + \frac{1}{\beta_c} \right)} \quad (4)$$

Tafel constants that are the anodic beta ( $\beta_a$ ) and cathodic beta ( $\beta_c$ ), and  $i_{corr}$  is corrosion current and B is a constant. The result is shown in Table (2), the polarization resistance ( $R_p$ ). Following, the equation of the corrosion rates (CR) is of the form.

$$CR = \frac{AW i_{corr} t}{n \rho A F} \quad (5)$$

Where, AW is atomic weight, for pure aluminum is 27 g/mol, because this element prevails in this alloy; n is the electron number involved in the reaction ( $Al^{+3}$ ); A is the electrode area ( $cm^2$ ); F is a constant Faraday (96487 Coulomb) and t time in year (31536000 s).

macropolarization technique was carried out, for this,  $\pm 150$  mV. This technique provides information about cathodic and anodic reactions on the sample surface, whose Tafel constants  $\beta$  and  $\beta$  were calculated and the result is presented in [Figure 7](#), besides, the corrosion current ( $i_{corr}$ ) [Toshev and Kostadinov \(2006\)](#) affirmed, which high corrosion rates are characterized by a small passive potential range and a lower pitting potential.

[Table 2](#) shows that the electrode at NaCl has a nobler behavior OCP than any in other solutions, meanwhile, the electrode at sodium hydroxide is less noble, this is in thermodynamic conditions. The cathodic polarization response of the electrode in NaCl shows higher reactivity compared to other solutions ([Figure 7](#)), however, the electrode at sodium hydroxide is less reactive, this is according to the dynamic conditions.

According to [Table 2](#), the corrosion-resistant behavior is due to a combination of corrosion potential shift in noble direction ( $E_{corr}$ ) and a lower corrosion current density ( $i_{corr}$ ). In particular, the workpiece in NaCl that simulates the seawater exhibits the noblest shift in  $E_{corr}$  (-0.213 V) and lowest  $i_{corr}$  ( $1.9 \times 10^{-7} A cm^{-2}$ ) and agreement with [Figure 7](#). Therefore, the sample in NaCl displays the smallest corrosion rate as shown in [Table 2](#). It is also evident that the workpiece in NaOH showed slightly

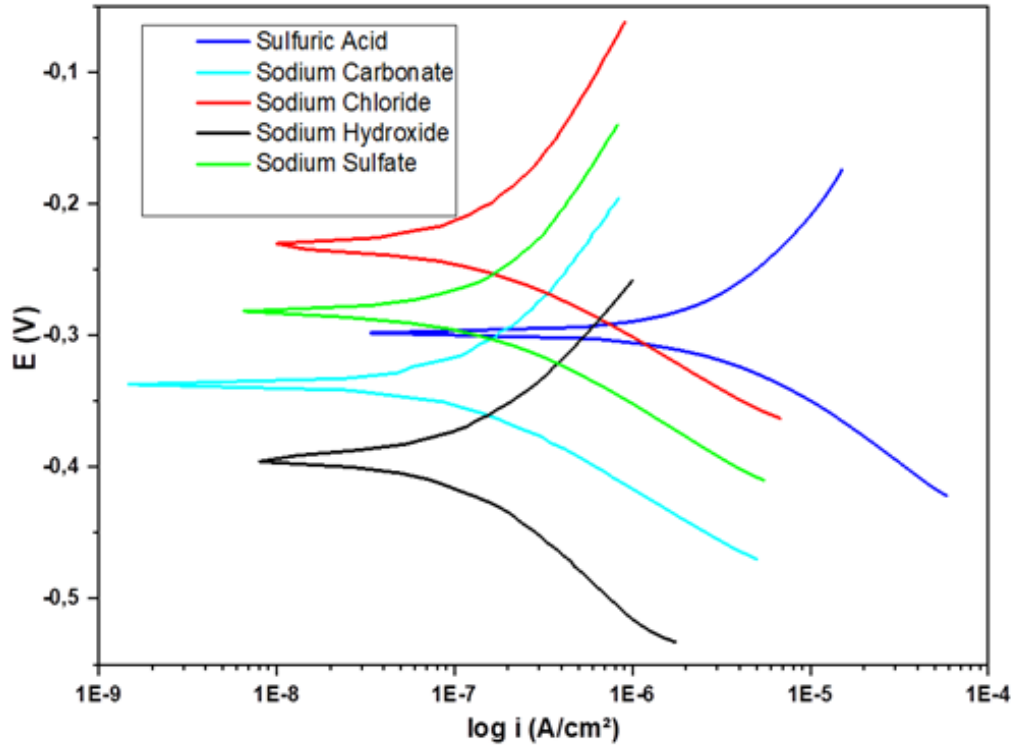


**Figure 7** Macropolarization curve at different electrolytes in BDSS workpiece

**Table 2** Electrochemical parameters of BDSS at different electrolytes alkaline and acidic mediums

	$E_{corr}$ [V]	$R_p$ [k $\Omega$ ]	$R_p.A$ [K $\Omega.cm^2$ ]	$\beta_a$ [V/dec]	$\beta_c$ [V/dec]	$I_{corr}$ [A] $\times 10^{-9}$	$I_{corr}/A$ [A/cm $^2$ ] $\times 10^{-7}$	CR [mm/year]
H <sub>2</sub> SO <sub>4</sub>	-0.272	406.2	75.959	0.97	0.123	0.579	3.1	0.0036
Na <sub>2</sub> SO	-0.26	578.8	108.235	0.178	0.084	0.428	2.3	0.0027
NaCl	-0.213	696.5	13.052	0.189	0.081	0.353	1.9	0.0023
Na <sub>2</sub> CO	-0.32	737.9	138.282	0.145	0.081	0.306	1.6	0.0019
NaOH	-0.382	635.1	119.018	0.141	0.126	0.442	2.4	0.0028

high  $i_{corr}$  ( $2.4 \times 10^{-7} A cm^{-2}$ ) and lowest  $E_{corr}$  (-0.382 V) values amongst the investigated solutions. Thus, the sample in NaCl displays the slightly high corrosion rate as shown in Table 2. So it can be emphasized, since the corrosion current density is directly proportional to the corrosion rate, a lower  $i_{corr}$  value generally signifies a higher corrosion-resistant behavior.

Concerning the study of duplex stainless steel corrosion, in the literature many authors have dealt about this subject, among them, Zanotto et al. [Zanotto et al. \(2015\)](#)

studied the phase transformation of the duplex stainless steel, which the conventional ferritic–austenitic duplex stainless steels (DSS) can be adversely affected by the precipitation and transformation phenomena in the 650–950 °C temperature range, this fact was verified in [Figure 1](#) by Thermo-Calc software, where various metastable phases arise in this temperature range, which is the most critical for the mechanical and corrosive behavior of these alloys. Still, these authors point out, the formation of chromium carbides and nitrides is possible at the ferrite ( $\alpha$ ) and austenite ( $\gamma$ ) grain boundaries also for brief time permanence in the 650–950 °C temperature range. In this work was confirmed that this fact does not present in this case, however, in this work came up principally boride phase, because the solidification speed is high in Spray Forming (SF) technical. Besides, [Aribo et al. \(2013\)](#) have reported that standard duplex and super duplex stainless steels exhibit good erosion-corrosion resistance due to their high hardness and the ability of the austenite phase of to harden under impingement. According to [Sousa et al. \(2010\)](#), the corrosion properties of both ferrite and austenite are dependent on the actual chemical composition. The main alloying elements, i.e., chromium, molybdenum, nickel, and nitrogen are not equally distributed in ferrite and austenite. Austenite is enriched with nickel and nitrogen, while, ferrite is enriched with chromium and molybdenum, which agrees with our discussion in section 3.2. It is clear that the chloride concentration exhibits a small influence on the corrosion resistance of the material; nevertheless, when included as an alloying element, Mo is incorporated into the passive film, producing oxides with different oxidation states and thus improves the pitting resistance of the stainless steel [Souza et al. \(2010\)](#). It has also been suggested by [Li et al. \(2016\)](#), which they found that the corrosion resistance of DSS is determined by the ratio of the  $\alpha$ -phase and  $\gamma$ -phase and by the Cr, Mo, and W depleted regions that are adjacent to the secondary phases. HDSS contains high levels of Cr, Mo, and N, resulting in its excellent corrosion resistance. Its excellent corrosion resistance properties rely on a well-balanced composition with approximately 50% ferrite ( $\alpha$ ) and 50% austenite ( $\gamma$ ) phases, that offer HDSS improved mechanical properties and higher chloride corrosion resistance compared with conventional DSS. The improved corrosion resistance extends the use of HDSS in more aggressive chloride environments, such as marine environments. Likewise, [Sánchez-Tovar et al. \(2015\)](#) remarked that DSS has a high resistance to both general and localized corrosion (specially to pitting and crevice corrosion in chloride-containing media) due to high chromium and molybdenum contents. Furthermore, [Meng et al. \(2007\)](#) attributed that erosion-corrosion behavior of the duplex stainless steels can be related to the volume fraction of the austenite phase and the flow rate of the slurry. However, [Hussain et al. \(2005\)](#) reported that for duplex stainless steel under Kuwait marine conditions, the extent to which the passivating film can assist in preventing erosion-corrosion.

### 3.6.3 ELECTROCHEMICAL IMPEDANCE SPECTROSCOPY

Electrochemical impedance spectroscopy (EIS) is another nondestructive technique to characterize electrochemical reactions at a corrosion interface. As a result of this study, Nyquist impedance plots is shown in [Figure 8](#) as the function of variation of the frequency (10 kHz to 100 Hz). The polarization resistance,  $R_p$ , is commonly used as a measure of the resistance of a metal to the corrosion damage. A high value of  $R_p$  is associated with a high corrosion prevention capability; a low value of  $R_p$  indicates potential high corrosion activity. Can be seen in this result, which these curves do not show the traditional curvature in Nyquist's diagram, being all have the linear behavior, so there is no way to measure the polarization resistance, besides that, according to this result, it means that the polarization resistance is very high for all solutions. In this diagram, it is observing the lowest linear angular coefficient corresponds to sodium hydroxide and the highest angular coefficient is for the sulfuric acid solution. According to the result of [Figure 8](#) for BDSS, the characteristic of the Nyquist impedance diagram was practically indifferent, either an acid or basic medium. In all these environments, the BDSS showed an extremely high resistance, this fact can be attributed mainly by the presence of the boron element or boride phases (M2B and M3B2) and among others meta-stable phases in the duplex stainless steel. This result was similar to the study carried out by authors [Zepon et al. \(2016\)](#).

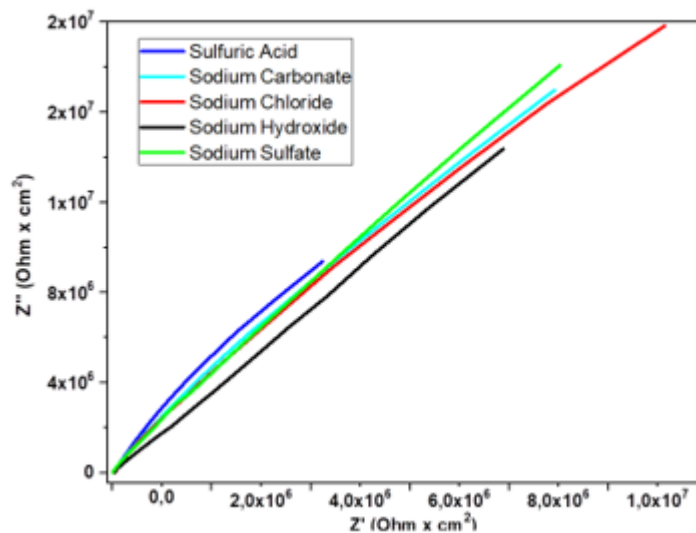


**Figure 8** Shows typical Nyquist impedance plots of BDSS workpiece at different electrolytes

To confirm this result will be confronted with different authors, among them, [Souza et al. \(2010\)](#) recommend that these features of extremely high resistance suggest a high degree of protection of the passive films formed, due to the presence of large amounts of chromium oxide. [Batista et al. \(2001\)](#) pointed out, the equivalent circuit is a way that can be proposed to simulate the

experimental results appropriately, but to propose the equivalent circuit involve many complexities, which required the semiconductor properties adequate of metallic oxides. Nevertheless, chromium nitrides may precipitate in duplex stainless steel during processing and their influence on the corrosion behavior is of great importance for the steel performance, as described by Bettini et al. [Bettini et al. \(2013\)](#). Chai and Kangas [Chai and Kangas \(2019\)](#) presented experimental results in extremely high critical pitting temperature, and critical crevice corrosion temperature of hyper duplex stainless steels allows the materials to be used in the areas where high corrosion resistance and high service temperature are required. The good combination of extra high strength and high ductility makes it possible for hyper duplex stainless steels to allow a substantial reduction in wall thickness, which leads to a reduction of weight in applications such as ultra-deep seawater, energy and refinery sectors. In all these situations the alloy's superior properties can be fully utilized to ensure reliability and safe service. Díaz et al. [del Coz Díaz et al. \(2010\)](#) confirmed that the high corrosion resistance and the excellent mechanical properties combination of duplex stainless steels can be explained by their chemical composition and balanced "duplex" microstructure of approximately equivalent volume fractions of ferrite and austenite. Firstly, the chemical composition based on high contents of Cr and Mo improves intergranular and pitting corrosion resistance, respectively. Moreover, additions of nitrogen can promote structural harden by an interstitial solid solution mechanism, which raises the yield strength and ultimate strength values without impairing toughness. Secondly, the two-phase microstructure guarantees higher resistance to pitting and stress corrosion cracking in comparison with conventional stainless steel. Duplex stainless steels are typically twice as strong as common austenitic stainless steels.

The workpiece of boron-modified duplex stainless steel with 2wt%B processed by spray-forming was studied by different technical, among them, microhardness test, corrosion behavior, and electrochemical impedance, therefore, following results were observed. High microhardness; high corrosion rates (CR) in different electrolytes alkaline and acidic mediums calculated by Tafel constants; furthermore, high polarization resistance ( $R_p$ ) calculated by Nyquist impedance plots. These results can be explained appropriately since this material was processed by Spray-Forming technical and this technique promotes refined microstructures with low segregation level, supersaturated solid solutions with meta-stable phases or even the formation of amorphous phases and optimal results of this study can mainly be attributed to the existence of borides of type  $(FeCr)_2B$ , which were verified by XRD spectra and Thermo-Calc software [Software \(2017\)](#), though, in this study has been stipulated approximately at 30% boride embedded in a matrix composed by austenite and ferrite in around equal fractions. All these results were corroborated by the literature presented in this work.

The applications of BDSS are so extensive in the industrial area, especially where there are very aggressive electrolyte media, as well as, allied with high temperatures

and pressure, which leads to a good combination of extremely high corrosion resistance and strength, the boron-modified duplex stainless steel can be successfully used in oil and gas extreme environments, in the ultra-deep formations or deep water wells. However, Díaz et al. [del Coz Díaz et al. \(2010\)](#) and Chai and Kangas [Chai and Kangas \(2019\)](#) pointed out that duplex stainless steels are finding major application in the chemical, oil and gas industries, petrochemical process plants, the pulp and paper industry, pollution control equipment, transportation and for general engineering thanks to their outstanding corrosion resistance and mechanical properties.

#### **4. CONCLUSION**

The following conclusions have been drawn from this investigation of the boron-modified duplex stainless steel with 2 wt%B processed by spray-forming:

1. In the ferrite phase, the Cr element predominates, but in the austenite phase the Fe and Ni elements prevail and (FeCr)<sub>2</sub>B phase is present,
2. XRD spectra and Thermo-Calc software of the boron-modified duplex stainless steel shown different ferrite, austenite, and (FeCr)<sub>2</sub>B phases.
3. Vickers microhardness measurements was around 460 HV being much higher than the duplex stainless steel and it can be attributed to the presence of (FeCr)<sub>2</sub>B phase and meta-stable phases.
4. Nyquist impedance plots for BDSS at different electrolytes in the function of variation of the frequency, all results had the linear behavior, it means that the polarization resistance is very high in all solutions.
5. The potential of corrosion whose magnitude is small, also the corrosion rates were very close to zero allied with high polarization resistance. Consequently, the corrosion resistance in the environment alkaline and acidic mediums were extremely high.
6. The excellent property of the material studied could be attributed to the presence of fine and well-distributed boride particles between the austenitic-ferritic matrix and due to a similar proportion of the three phases present.
7. The BDSS can be successfully used in the oil and gas extreme environments in the ultra-deep formations or deep-water wells, in the chemical, oil and gas industries, petrochemical process plants, the pulp and paper industry, pollution control equipment and transport tanks.

#### **5. ACKNOWLEDGMENTS**

This work was entirely financed by CNPq (Brazilian National Council for Scientific and Technological Development), FINEP (Research and Projects Financing Agency), and to LABMU-UEPG laboratory.

## REFERENCES

- Aribo, S., Barker, R., Hu, X., & Neville, A. (2013). Erosion–corrosion behaviour of lean duplex stainless steels in 3.5% NaCl solution. *Wear*, 302(1-2), 1602–1608. Retrieved from <https://dx.doi.org/10.1016/j.wear.2012.12.007> 10.1016/j.wear.2012.12.007
- Arun, D., Ramkumar, K. D., & Vimala, R. (2019). Multi-pass arc welding techniques of 12 mm thick super-duplex stainless steel. *Journal of Materials Processing Technology*, 271, 126–143. Retrieved from <https://dx.doi.org/10.1016/j.jmatprotec.2019.03.031> 10.1016/j.jmatprotec.2019.03.031
- Bastidas, J. M., Polo, J. L., Torres, C. L., & Cano, E. (2001). A study on the stability of AISI 316L stainless steel pitting corrosion through its transfer function. *Corrosion Science*, 43(2), 269–281. Retrieved from [https://dx.doi.org/10.1016/s0010-938x\(00\)00082-2](https://dx.doi.org/10.1016/s0010-938x(00)00082-2) 10.1016/s0010-938x(00)00082-2
- Bastos, I. N., Tavares, S. S., Dalard, F., & Nogueira, R. P. (2007). Effect of microstructure on corrosion behavior of superduplex stainless steel at critical environment conditions. *Scripta Materialia*, 57(10), 913–916. Retrieved from <https://dx.doi.org/10.1016/j.scriptamat.2007.07.037> 10.1016/j.scriptamat.2007.07.037
- Bettini, E., Kivisäkk, U., Leygraf, C., & Pan, J. (2013). Study of corrosion behavior of a 22% Cr duplex stainless steel: Influence of nano-sized chromium nitrides and exposure temperature. *Electrochimica Acta*, 113, 280–289. Retrieved from <https://dx.doi.org/10.1016/j.electacta.2013.09.056> 10.1016/j.electacta.2013.09.056
- Chai, G., & Kangas, P. (2019). Hyper-Duplex Stainless Steels. *Hyper-Duplex Stainless Steels*. Retrieved from [https://www.Materials.Sandvik/Contentassets/2fb9a78a95e54cfba303361e04151a68/Sav0049\\_Whitepaper\\_Hyperduplex\\_150606.Pdf.2017.Accessed11November](https://www.Materials.Sandvik/Contentassets/2fb9a78a95e54cfba303361e04151a68/Sav0049_Whitepaper_Hyperduplex_150606.Pdf.2017.Accessed11November)
- Chail, G., & Kangas, P. (2016). Super and hyper duplex stainless steels: structures, properties and applications. *Procedia Structural Integrity*, 2, 1755–1762. Retrieved from <https://dx.doi.org/10.1016/j.prostr.2016.06.221> 10.1016/j.prostr.2016.06.221
- Charles, J., & Bernhardsson, S. (1991). Super Duplex Stainless Steels: Structure And Properties. In V. E. Charles & J. (Eds.), *Duplex Stainless Steels'91* (pp. 3–48).
- del Coz Díaz, J. J., Rodríguez, P. M., Nieto, P. J. G., & Castro-Fresno, D. (2010). Comparative analysis of TIG welding distortions between austenitic and duplex stainless steels by FEM. *Applied Thermal Engineering*, 30(16), 2448–2459. Retrieved from <https://dx.doi.org/10.1016/j.applthermaleng.2010.06.016> 10.1016/j.applthermaleng.2010.06.016
- Deng, B., Wang, Z., Jiang, Y., Sun, T., Xu, J., & Li, J. (2009). Effect Of Thermal Cycles On The Corrosion And Mechanical Properties Of Uns S31803 Duplex Stainless Steel. *Corrosion Science*, 51, 2969–2975.
- Emami, S., Saeid, T., & Khosroshahi, R. A. (2018). Microstructural evolution of friction stir welded SAF 2205 duplex stainless steel. *Journal of Alloys and Compounds*, 739, 678–689. Retrieved from <https://dx.doi.org/10.1016/j.jallcom.2017.12.310> 10.1016/j.jallcom.2017.12.310
- Hussain, E., & Husain, A. (2005). Erosion — corrosion of duplex stainless steel under Kuwait marine condition. *Desalination*, 183(1-3), 227–234. Retrieved from <https://dx.doi.org/10.1016/j.desal.2005.02.051> 10.1016/j.desal.2005.02.051
- Kashiwar, A., Vennela, N. P., Kamath, S. L., & Khatirkar, R. K. (2012). Effect of solution annealing temperature on precipitation in 2205 duplex stainless steel. *Materials Characterization*, 74, 55–63. Retrieved from <https://dx.doi.org/10.1016/j.matchar.2012.09.008> 10.1016/j.matchar.2012.09.008

- Li, H., Zhou, E., Zhang, D., Xu, D., Xia, J., Yang, C., Feng, H., Jiang, Z., Li, X., Gu, T., & Yang, K. (2016). Microbiologically Influenced Corrosion Of 2707 Hyper-Duplex Stainless Steel By Marine *Pseudomonas Aeruginosa* Biofilm. *Scientific Reports*.
- Martins, M. (2006). Microstructural-Mechanical Characterization And Corrosion Resistance Of Astm A890 / A890m Grade 6a Super Duplex Stainless, Doctoral Thesis, Universidade De São Paulo-Br, Interunidades Eesc-Ifsc-Iqsc, Steel. *Microstructural-Mechanical Characterization And Corrosion Resistance Of Astm A890 / A890m Grade 6a Super Duplex Stainless*.
- Martins, M., & Casteletti, L. C. (2005). Heat treatment temperature influence on ASTM A890 GR 6A super duplex stainless steel microstructure. *Materials Characterization*, 55(3), 225–233. Retrieved from <https://dx.doi.org/10.1016/j.matchar.2005.05.008> 10.1016/j.matchar.2005.05.008
- Meng, H., Hu, X., & Neville, A. (2007). A systematic erosion–corrosion study of two stainless steels in marine conditions via experimental design. *Wear*, 263(1-6), 355–362. Retrieved from <https://dx.doi.org/10.1016/j.wear.2006.12.007> 10.1016/j.wear.2006.12.007
- Mironova-Ulmane, N., Kuzmin, A., Sildos, I., & Pärns, M. (2011). Polarisation dependent Raman study of single-crystal nickel oxide. *Open Physics*, 9(4). Retrieved from <https://dx.doi.org/10.2478/s11534-010-0130-9> 10.2478/s11534-010-0130-9
- Pehkonen, S. O., & Yuan, S. (2019). Tailored Thin Coatings For Corrosion Inhibition Using A Molecular Approach. *Interface Science And Technology*, 23.
- Ran, Q., Liu, Q., Xu, Y., Xu, W., Li, J., Xiao, X., Hu, J., & Jiang, L. (2015). Nitrogen-Induced Selective High-Temperature Internal Oxidation Behavior In Duplex Stainless Steels. *Nitrogen-Induced Selective High-Temperature Internal Oxidation Behavior In Duplex Stainless Steels 19cr-10mn-0.3ni-xn*, 98, 737–747.
- Sánchez-Tovar, R., Leiva-García, R., & García-Antón, J. (2015). Characterization of thermal oxide films formed on a duplex stainless steel by means of confocal-Raman microscopy and electrochemical techniques. *Thin Solid Films*, 576, 1–10. Retrieved from <https://dx.doi.org/10.1016/j.tsf.2014.12.024> 10.1016/j.tsf.2014.12.024
- Sharafi, S. (1993). Microstructure Of Super-Duplex Stainless Steels. Doctor Of Philosophy. St. Edmund College, The University Of Cambridge. *Microstructure Of Super-Duplex Stainless Steels. Doctor Of Philosophy*. Retrieved from <https://doi.org/10.17863/Cam.14216>
- Smuk, O. (2004). Microstructure And Properties Of Modern P/M Super Duplex Stainless Steels. Doctoral Thesis. Dpto Of Materials Science And Engineering, Royal Institute Of Technology. *Microstructure And Properties Of Modern P/M Super Duplex Stainless Steels. Doctoral Thesis. Dpto Of Materials Science And Engineering*.
- Software, T.-C. (2017). Stockholm. Stockholm, Sweden.
- Souza, E. C., Rossitti, S. M., & Rollo, J. M. (2010). Influence of chloride ion concentration and temperature on the electrochemical properties of passive films formed on a superduplex stainless steel. *Materials Characterization*, 61(2), 240–244. Retrieved from <https://dx.doi.org/10.1016/j.matchar.2009.12.004> 10.1016/j.matchar.2009.12.004
- Soyama, J., Lopes, T. P., Zepon, G., Kiminami, C. S., Botta, W. J., & Bolfarini, C. (2019). Wear Resistant Duplex Stainless Steels Produced by Spray Forming. *Metals and Materials International*, 25(2), 456–464. Retrieved from <https://dx.doi.org/10.1007/s12540-018-0202-8> 10.1007/s12540-018-0202-8
- Standard Practice For Castings, Iron-Chromium-Nickel-Molybdenum Corrosion Resistant,

- Duplex (Austenitic/Ferritic) For General Application. (1999). In *American Society For Testing And Materials - Astm A890/A890m-91* (pp. 556–569). Annual Book Of Astm Standards.
- Toshev, Y., Kostadinov, K., & K. (2006). Protective Coating Of Zinc And Zinc Alloys For Industrial Applications. *4m 2006 - Second International Conference On Multi-Material Micro Manufacture*, 397–326.
- Wang, S., Ma, Q., & Li, Y. (2011). Characterization Of Microstructure, Mechanical Properties And Corrosion Resistance Of Dissimilar Welded Joint Between 2205 Duplex Stainless Steel And 16mnr. *Materials And Design*, 32, 831–837.
- Xu, Y., Jin, Q., Li, J., Xiao, X., & Zhang, X. (2012). Oxidation Induced Phase Transformation Of Duplex Stainless Steel 25cr-10mn-2ni. *Corrosion Science*, 55, 233–237.
- Zanotto, F., Grassi, V., Merlin, M., Balbo, A., & Zucchi, F. (2015). Effect of brief heat treatments performed between 650 and 850°C on corrosion behaviour of a lean duplex stainless steel. *Corrosion Science*, 94, 38–47. Retrieved from <https://dx.doi.org/10.1016/j.corsci.2015.01.035> 10.1016/j.corsci.2015.01.035
- Zepon, G., Ellendt, N., Uhlenwinkel, V., & Bolfarini, C. (2016). Solidification Sequence of Spray-Formed Steels. *Metallurgical and Materials Transactions A*, 47(2), 842–851. Retrieved from <https://dx.doi.org/10.1007/s11661-015-3253-1> 10.1007/s11661-015-3253-1